Available online at www.sciencedirect.com
ScienceDirect
International Journal of Thermal Sciences 47 (2008) 442–449
International Journal of Thermal Sciences
www.elsevier.com/locate/ijts

Forced convection heat transfer from banks of helical coiled resistance wires

G. Comini [a,*], S. Savino [a], E. Bari [b], A. Bison [b]

[a] *University of Udine, Department of Energy and Fluid Machinery, Via delle Scienze 208, 33100 Udine, Italy*
[b] *Electrolux Home Products Italy Spa, Corso Lino Zanussi 30, 33080 Porcia (PN), Italy*

Received 6 June 2006; received in revised form 12 March 2007; accepted 13 March 2007

Available online 26 April 2007

Abstract

Forced convection heat transfer from banks of helical coiled resistance wires in a cross flow of air was investigated experimentally, with reference to various operative conditions and several coil geometries. The resistance banks were subdivided in two branches, independently powered by single-phase alternating current. Average convection heat transfer coefficients were determined for each branch. No significant interactions were detected between adjacent coils nor between upstream and downstream coils, possibly because of the high percentage of inter-spaces between wires. The experimentally measured Nusselt numbers were thus correlated by a modified version of the Churchill and Bernstein model, valid for a single cylinder in cross flow. To this purpose, an equivalent wire diameter was defined in order to take into account the influences of diameter and pitch of the coils. The average deviation between measured and calculated values of the Nusselt number is of the order of $\pm 7\%$ in the range of Reynolds numbers from 70 to 400.

Keywords: Electric heating; Helical coils; Banks of resistance wires; Forced convection; Cross flow

1. Introduction

Helical coiled resistance wires are among the most cost-effective solutions for many home and industrial appliances which utilize electric air heating. The open-coil construction is less expensive than the finned-tubular construction and, for the same heating power, leads to a quicker thermal response and a lower pressure drop. The only draw-back is that the open-coil construction cannot be utilized if foreign particles contaminate the air flow to the point of obstructing the inter-coil spaces [1]. On the contrary, the open-coil solution is technically appropriate if the air flow is filtered, as it happens in many situations of industrial interest.

Despite the widespread use of open-coil air heaters, forced convection heat transfer from helical coiled resistance wires in cross flow has not been considered in the literature. Many studies are available on forced convection heat transfer from straight cylinders in cross flow (see, for example, Ref. [2]), and on forced convection heat transfer from banks of straight tubes in cross flow (see, for example, Ref. [3]). Conversely only some loosely related information, concerning natural convection heat transfer, can be found for helical coiled tubes [4–8]. The aim of the present study is to partially fill this informative gap, investigating forced convection heat transfer in cross flow from banks of open-coil resistance wires of the type utilized in tumble dryer appliances.

The measurements concerned four coil geometries and a wide range of operative conditions. The experimental procedure was focused on the evaluation of average convection heat transfer coefficients, and the experimental data were correlated in terms of Reynolds number (Re), Prandtl number (Pr), and average Nusselt number $\overline{Nu}$. To this aim the Churchill and Bernstein correlation, valid in the semi-infinite interval: $Re\,Pr > 2$ [9], was modified to take into account the influence of the coil geometry through the introduction of an equivalent wire diameter.

2. Experimental apparatus and test procedures

The open-circuit wind tunnel utilized in this research is schematized in Fig. 1. The centrifugal blower is driven by a

* Corresponding author. Tel.: +39 0432 558023; fax: +39 0432 558027.
E-mail address: gianni.comini@uniud.it (G. Comini).

1290-0729/$ – see front matter
doi:10.1016/j.ijthermalsci.2007.03.009

Nomenclature

a	thermal diffusivity	m^2/s
A	area	m^2
Bi	Biot number, $=\alpha d/\lambda_w$	
c_p	fluid specific heat	J/(kg K)
d	wire diameter	m
D	coil diameter	m
d_0	reference diameter [Eq. (24)]	m
E	supply voltage	V
H	height	m
I	load current	A
L	length	m
Nu	Nusselt number, $=\alpha d_0/\lambda_f$	
p	pressure	Pa
P	electric power	W
Pr	Prandtl number, $=\nu/a$	
q	heat flow rate	W
q''	heat flux	W/m^2
r	electric resistivity	Ω m
R	electric resistance	Ω
Re	Reynolds number, $=\bar{u}d_0/\nu$	
S_C	pitch of the coil helix	m
S_L	longitudinal distance between coils	m
S_T	transverse distance between coils	m
t	relative temperature	°C
T	absolute temperature	K
$\bar{u}$	average velocity	m/s
$\dot{V}$	volume flow rate	m^3/s
W	width	m
(x, y, z)	Cartesian coordinates	m
X	electric reactance	Ω
Z	electric impedance	Ω

Greek symbols

α	convection heat transfer coefficient	$W/(m^2 K)$
β	temperature coefficient of resistance	1/K
ϵ	emissivity	
λ	thermal conductivity	W/(m K)
ν	kinematic viscosity	m^2/s
ρ	fluid density	kg/m^3
σ	Stefan–Boltzmann constant	$W/(m^2 K^4)$

Subscripts

0	reference conditions
avr	averaged over a set
C	coil
c	convection
d	duct
e	experimental
f	fluid
i	inlet
o	outlet
r	radiation
R	reversed
s	surface
S	support
u	unobstructed
w	wire

Overbar

$\bar{}$	average value

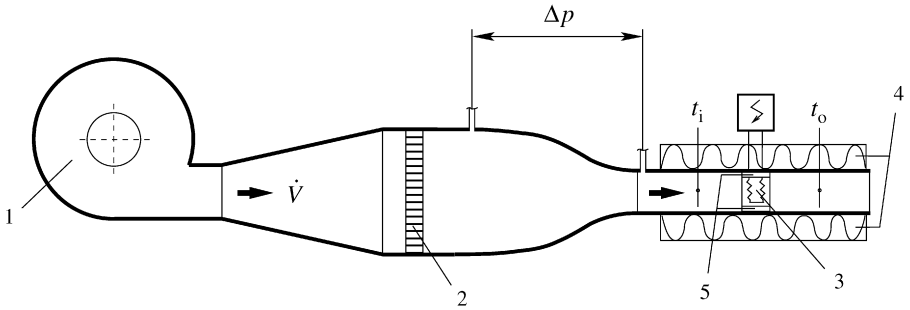

Fig. 1. Schematization of the open-circuit wind tunnel: (1) centrifugal fan, (2) honeycomb, (3) working section, (4) external fiberglass insulation and (5) distance spacers (not to scale).

variable-speed motor, and takes air from a large laboratory room, thermostated within ±0.5 K. The blower discharges to a diffuser, which is followed by a honeycomb and a contraction. The combination of diffuser, honeycomb and contraction limits the velocity variations and the turbulence levels in the working section. Several distance spacers in Teflon, placed along the flow direction, produce a very thin flow passage (about 1 mm thick) between the heater-case and the inside of the duct. In this way, contact areas and thermal bridges are significantly reduced, and a "dynamic insulation" effect is produced by the very limited amount of air flowing through the gap. The working section is externally insulated with a 8 cm layer of fiberglass. The combination of spacers, guard-heater gap and external insulation limits heat losses to the point that external temperatures of the insulation coincide, within the instrumental accuracy of ±0.2 K, with the room temperature. The volume flow rate of air $\dot{V}$ is changed by varying the rotational speed of the centrifugal fan, and is monitored through the pressure

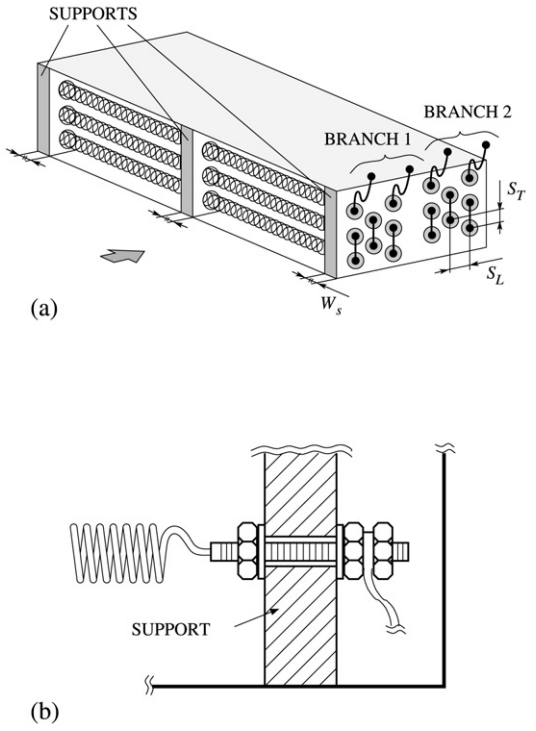

Fig. 2. Schematizations of (a) the heater and (b) the terminal box for the cable leads.

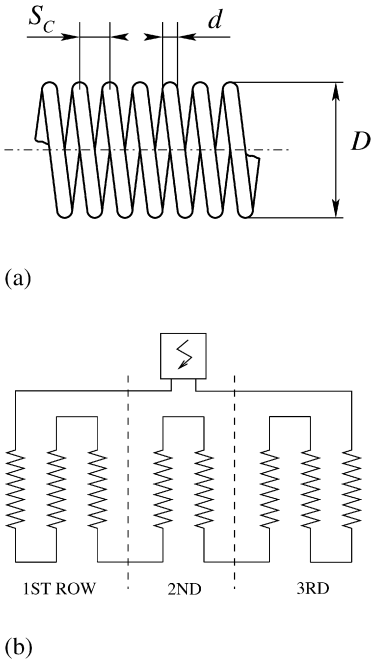

Fig. 3. Schematizations of (a) the coil geometry and (b) the electric connections in a branch.

Table 1
Geometric and electric characteristics of the branch 1 and the branch 2 of the heaters A and B utilized in the tests

Branch	A1	A2	B1	B2
Rated power P [W]	1000	1400	600	1400
Wire diameter $d \cdot 10^3$ [m]	0.60	0.65	0.5	0.65
Coil diameter $D \cdot 10^3$ [m]	6.0	6.0	7.0	7.0
Pitch of the coil helix $S_C \cdot 10^3$ [m]	1.58	1.87	1.70	2.37
Number of coil turns	720	608	668	480
Total length of the coil L_C [m]	13.6	11.5	14.7	10.6
Heat exchange area $A \cdot 10^2$ [m^2]	2.56	2.34	2.31	2.15
Longitudinal distance between coils $S_L \cdot 10^2$ [m]	1.35	1.35	1.35	1.35
Transverse distance between coils $S_T \cdot 10^2$ [m]	1.05	1.05	1.05	1.05
Rated load q'' [kW/m^2]	39	60	26	65
Reference electric resistance R_0 [Ω]	50.6	36.2	77.5	33.2

difference Δp between the piezometer tappings located at inlet and outlet of the contraction. The differential pressure signal is picked-up continuously by an electronic gauge. The calibration curve ($\dot{V}$ vs. Δp) of the gauge was obtained by preliminary measurements in which an obstruction meter of the nozzle type substituted the resistance bank.

The duct heaters are schematized in Fig. 2. As can be seen from Fig. 2(a), the bank of resistances is subdivided in two branches: an upstream branch 1 and a downstream branch 2. It is worth noting that, during the preliminary tests, the heat transfer performances did not significantly change when the direction of the flow was reversed by rotating the heaters, so as to have branch 2 upstream and branch 1 downstream. In Section 4 it will be shown that this finding can be interpreted as an indication of the negligible role played by the wake interactions between coils.

The coils are held in position by three, mica-ceramic supports of thickness $W_S = 5$ mm that are mechanically fixed to the heater case. The distances between coils in each branch are S_L in the longitudinal direction and S_T in the transverse direction. A lateral terminal box, of the type schematized in Fig. 2(b), provides the necessary space for the cable leads. The geometry of a coil, illustrated in Fig. 3(a), shows how a wire of diameter d is bended into a helix of pitch S_C and diameter D. The coils are made of Nikrothal 40, an alloy whose composition is: 20% Cr, 45% Fe and 35% Ni. The electric connections within each branch are schematized in Fig. 3(b). Because of the series connections, the reference value R_0 of the total electric resistances at 0 °C, supplied by the manufacturer, corresponds to the sum of the eight resistances in each branch. Two geometrically different heaters, indicated as A and B, were extensively tested. Four heating loads A1, A2, B1 and B2, were obtained by switching on the branch 1 or the branch 2 of the heater A or of the heater B, respectively. The heating loads (A1 + A2) and (B1 + B2) were not considered, since average temperatures $\bar{t}_s$ of a heating elements can be reasonably defined only for a single branch. The geometric and electric characteristics of the heaters are reported in Table 1.

During the tests, the supply voltage E is regulated by a variable transformer and is measured by a voltmeter, while the resulting load current I is measured by an ammeter. The input power to the branch can be conveniently evaluated as

$$P = EI\cos\phi \cong EI \tag{1}$$

where $\cos\phi \cong 1$ is the power factor. The assumption: $\cos\phi \cong 1$ is fully justified since, in the coils considered, the ratios X/R between reactances X and resistances R are of the order of

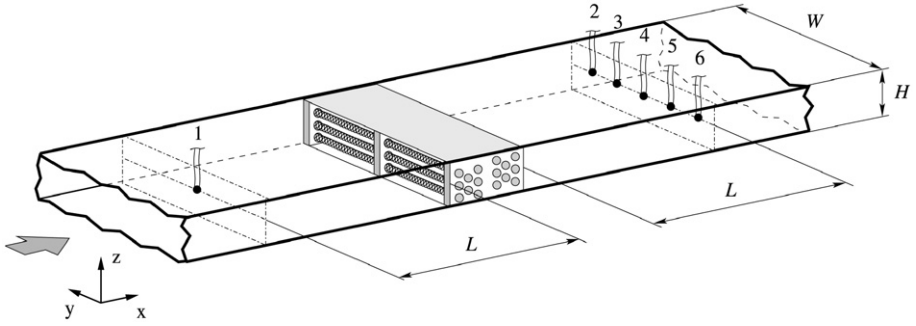

Fig. 4. Working section and position of the measuring thermocouples.

0.1%. Consequently, $\cos\phi$ does not significantly differ from 1 and the impedance of the coils

$$Z = \sqrt{R^2 + X^2} \cong R \tag{2}$$

does not significantly differ from the resistance R. Preliminary assessments, based on wattmeter readings in addition to the already mentioned voltmeter and ammeter readings, fully supported these assumptions.

2.1. Average fluid velocity and temperatures

The average fluid velocity in the working section is calculated as

$$\bar{u} = \dot{V}/A_u \tag{3}$$

with reference to the unobstructed area of the channel A_u. In the working section, illustrated in Fig. 4, the width W and height H of the channel are 157 mm and 43 mm, respectively. In correspondence with the heater, however, about 9.5% of the flow passage is obstructed by the ceramic supports and the distance spacers. The area of the unobstructed cross section can thus be evaluated as $A_u = 0.905WH$, yielding $A_u = 61 \cdot 10^{-4}$ m^2.

Fluid temperatures are monitored at several locations along the test section by means of calibrated copper-constantan thermocouples. The measuring thermocouples are positioned at equal distances $L = 0.14$ m upstream and downstream of the heater. This value of L was chosen as the best compromise between reduction of external heat losses (which increase with L), and reduction of direct thermal radiation from the resistance wires (which decreases with L). As can be seen, there is a single measuring point at inlet, where the temperature t_i is uniform within instrumental accuracy. On the contrary, there are five measuring points at outlet, where the temperature t_o is strongly influenced by the flow separation downstream of the central support [10].

A computer-based data acquisition system records all the experimental measurements. Temperature vs. time recordings are shown in Fig. 5(a) with reference to a typical run. In the tests it was assumed that steady state was reached when time oscillations of the outlet temperatures remained in the ± 0.5 K interval. Temperatures were evaluated in this pseudo-steady state, by time-averaging the recorded levels over a 10 min period. Space distributions of time-averaged temperatures at outlet behaved as shown in Fig. 5(b), presenting the expected peaks downstream of the central partition [10].

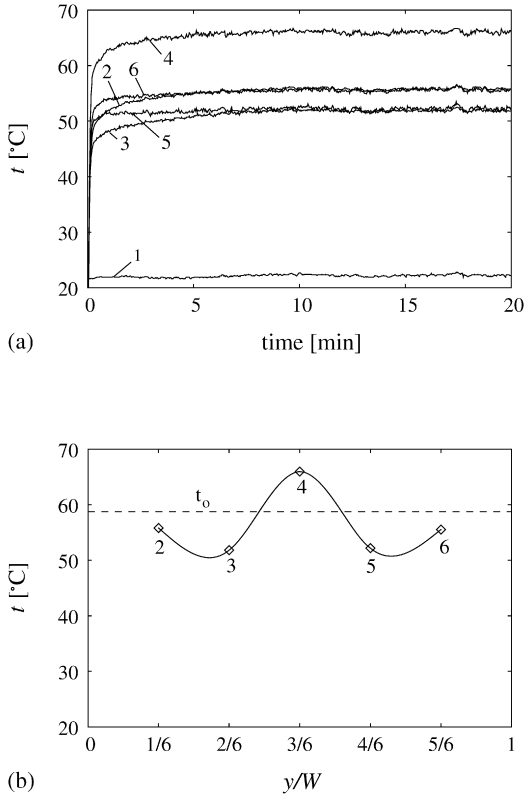

Fig. 5. Time behavior of measured temperatures (a) and time-averaged temperatures at outlet in the stabilized phase (b) of a typical run.

In situations of thermal equilibrium with negligible external heat losses, the whole electric power P is transferred to the air stream, either directly (by convection heat transfer from the resistances) or indirectly (by radiation heat transfer from the resistances to the duct, followed by convection heat transfer from the duct to the air stream). We have thus

$$P = q_c + q_r \tag{4}$$

and the bulk temperature of the air stream at outlet can be calculated as

$$t_o = t_i + \frac{P}{\rho c_p \dot{V}} \tag{5}$$

where $\dot{V}$ is the volume flow rate, and ρ and c_p are evaluated at the average fluid temperature

$$\bar{t}_f = (t_i + t_o)/2 \tag{6}$$

between inlet and outlet.

2.2. Average coil temperatures

Average coil temperatures $\bar{t}_s$ cannot be directly measured, since the diameter of the resistances is comparable with the diameter of the thermocouples. The evaluation of coil temperatures was thus based on the relationship between electric resistivity r and temperature t. In the temperature range from 0 °C to 300 °C, the resistivity of the Nikrothal 40 alloy can be expressed as

$$\frac{r(t)}{r_0} = 1 + \beta t \tag{7}$$

where $r(t)$ is the resistivity at the temperature t, r_0 is the resistivity of reference, evaluated at the temperature of 0 °C, and β is the temperature coefficient. By disregarding the variations with temperature of the geometric characteristics of the wires, the resistivity ratio at the average coil temperature t_s can be estimated from the corresponding ratio of total electric resistances

$$\frac{R(\bar{t}_s)}{R_0} \cong \frac{r(\bar{t}_s)}{r_0} = 1 + \beta \bar{t}_s \tag{8}$$

where $R(\bar{t}_s)$ is the resistance at the average coil temperature $\bar{t}_s$, and R_0 is the resistance at the reference temperature of 0 °C. Finally, under the assumptions: $X \ll R$ and $\cos\phi \cong 1$, the electric resistance can be evaluated as

$$R = E/I \tag{9}$$

from voltmeter and ammeter readings.

For the coils utilized in this study the $R(\bar{t}_s)/R_0$ vs. $\bar{t}_s$ curve, plotted in Fig. 6, was obtained from a series of preliminary measurements made at various temperatures in a thermostated oven. After reaching thermal equilibrium, in fact, the temperature and the corresponding electric resistance are easily measured. It is worth noticing that the $R(\bar{t}_s)/R_0$ vs. $\bar{t}_s$ curve did not depend on the particular coil tested. A single value for the temperature coefficient of the material $\beta = 3.37 \cdot 10^{-4}$ K^{-1} was thus used for all the coils.

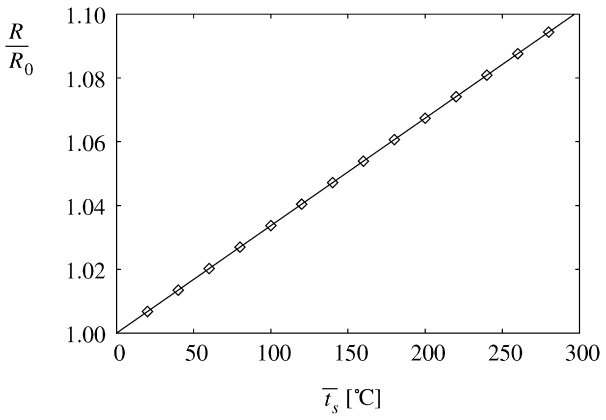

Fig. 6. Variation of the electric resistance with temperature.

2.3. Average convection heat transfer coefficient

In accordance with the experimental procedure employed in this study, the average convection heat transfer coefficient was defined as

$$\bar{\alpha} = \frac{q_c}{A(\bar{t}_s - \bar{t}_f)} \tag{10}$$

where $\bar{t}_f$ is the average temperature of the fluid, yielded by Eq. (6), $\bar{t}_s$ is the average temperature of the heating resistances estimated from Eq. (8), and A is the area of the coils.

The convective heat flow rate from the resistances to the air stream was evaluated on the basis of Eq. (4), written in the form

$$q_c = P - q_r \tag{11}$$

The radiation contribution

$$q_r = \epsilon\sigma A\left(\bar{T}_s^4 - T_d^4\right) \tag{12}$$

was evaluated from the known value of the emissivity of Nikrothal 40 ($\epsilon = 0.88$), the measured value of the absolute coils temperature: $\bar{T}_s = \bar{t}_s + 273.15$, and the estimated value of the absolute duct temperature: $T_d \cong T_f = \bar{t}_f + 273.15$.

3. Uncertainty analysis

The uncertainty in the evaluation of a variable V, which is a known function of n dependent variables v, can be expressed as [11, Chapter 3]

$$\Delta V = \left[\sum_{j=1}^{n}\left(\frac{\partial V}{\partial v_j}\Delta v_j\right)^2\right]^{1/2} \tag{13}$$

From the general relationship (13) it follows that [12, Chapter 3]

$$\frac{\Delta V}{V} = \frac{\Delta v}{v} \tag{14}$$

if $V = Cv$, with $C = const$;

$$\frac{\Delta V}{V} = \left[\left(\frac{\Delta v_1}{v_1}\right)^2 + \left(\frac{\Delta v_2}{v_2}\right)^2\right]^{1/2} \tag{15}$$

if $V = Cv_1v_2$ or $V = Cv_1/v_2$, and

$$\frac{\Delta V}{V} = \left[\frac{(\Delta v_1)^2 + (\Delta v_2)^2}{(v_1 \pm v_2)^2}\right]^{1/2} \tag{16}$$

if $V = v_1 \pm v_2$.

3.1. Uncertainty of main measurement items

First of all it must be noted that the fluid properties change slowly with temperature. Consequently, uncertainty in the evaluation of thermal properties can be disregarded with respect to the uncertainties of the main measurement items. In accordance with this assumption and on the basis of Eq. (15), the uncertainty in the evaluation of the average fluid velocity estimated as

$$\frac{\Delta\bar{u}}{\bar{u}} \cong \frac{\Delta\dot{V}}{\dot{V}} \tag{17}$$

is of the order of ±3%, since this is the relative uncertainty of the volume flow rate measurements.

As already noted, the uncertainty in the evaluation of t_i coincides with the uncertainty (±0.2 K) in the calibration of the thermocouples. Since the uncertainty in the evaluation of t_o from time- and space-averaged readings is of the order of ±4 K, it follows from Eq. (6) that the uncertainty in the evaluation of $\bar{t}_f$ is of the order of ±2 K.

The relative uncertainty of the $R(\bar{t}_s)/R_0$ vs. $\bar{t}_s$ curve, which is of the order of ±2%, leads to an uncertainty of about ±5 K in the evaluation of the coil temperatures $\bar{t}_s$. With respect to this value, we can neglect the additional uncertainty brought about by the evaluation of the oven temperature (±0.2 K in the temperature range from 0 and 300 °C).

The orders of magnitude in Eq. (11) are: $q_r/P \leqslant 0.1$, $q_c/P \geqslant 0.9$ and, consequently, $q_c/q_r \geqslant 9$. Thus, from Eq. (16) we obtain immediately

$$\frac{\Delta q_c}{q_c} = \left[\left(\frac{\Delta P}{q_c}\right)^2 + \left(\frac{\Delta q_r}{q_c}\right)^2\right]^{1/2} \cong \left[\left(\frac{\Delta P}{0.9P}\right)^2 + \left(\frac{\Delta q_r}{9\,q_r}\right)^2\right]^{1/2} \tag{18}$$

The relative uncertainty $\Delta q_r/q_r$ is of the order of ±30%, and the relative uncertainty $\Delta P/P$ is of the order of ±1%. Therefore, the relative uncertainty $\Delta q_c/q_c$ is of the order of ±3%.

3.2. Uncertainty of the experimental validation

In this research, the prediction model for $\bar{\alpha}$ is developed in terms of average Nusselt numbers, Reynolds numbers and Prandtl numbers. Since the validation involves a comparison with the experimental results, the estimation of the uncertainty in the evaluation of the experimentally measured $\overline{Nu}$, Re and Pr is of paramount importance.

As already pointed out, the fluid properties change slowly with temperature. Consequently, the uncertainty in the evaluation of the Prandtl number can be neglected. The relative uncertainty in the evaluation of the Reynolds number can be computed from the relationship

$$\frac{\Delta Re}{Re} = \frac{\Delta \bar{u}}{\bar{u}} \tag{19}$$

and, therefore, is of the order of ±3%.

The relative uncertainty in the evaluation of the average Nusselt number can be computed from the relationship

$$\frac{\Delta \overline{Nu}}{\overline{Nu}} = \frac{\Delta \bar{\alpha}}{\bar{\alpha}} \tag{20}$$

The uncertainty in the evaluation of the average convection heat transfer coefficient can be estimated from Eqs. (10) and (15) which yield

$$\frac{\Delta \bar{\alpha}}{\bar{\alpha}} = \left\{\frac{(\Delta q_c)^2}{(q_c)^2} + \frac{[\Delta(\bar{t}_s - \bar{t}_f)]^2}{(\bar{t}_s - \bar{t}_f)^2}\right\}^{1/2} \tag{21}$$

while, from Eq. (16), we have

$$\frac{\Delta(\bar{t}_s - \bar{t}_f)}{\bar{t}_s - \bar{t}_f} = \left[\frac{(\Delta \bar{t}_s)^2 + (\Delta \bar{t}_f)^2}{(\bar{t}_s - \bar{t}_f)^2}\right]^{1/2} \tag{22}$$

Since $\Delta q_c/q_c \cong \pm 3\%$, $\Delta \bar{t}_f \cong \pm 2$ K and $\Delta \bar{t}_s \cong \pm 5$ K, by assuming an average value of $(\bar{t}_s - \bar{t}_f) \cong 150$ K we obtain in sequence: $\Delta(\bar{t}_s - \bar{t}_f)/(\bar{t}_s - \bar{t}_f) \cong \pm 4\%$ and $\Delta \bar{\alpha}/\bar{\alpha} \cong \pm 5\%$.

4. Prediction model

In the prediction of forced convection heat transfer coefficients from a single cylinder in cross flow, the Churchill and Bernstein correlation

$$\overline{Nu} = 0.30 + \frac{0.62 Re^{1/2} Pr^{1/3}}{[1 + (0.40/Pr)^{2/3}]^{1/4}}\left[1 + \left(\frac{Re}{282\,000}\right)^{5/8}\right]^{4/5} \tag{23}$$

is widely used for Re and Pr numbers in the semi-infinite interval: $Re\,Pr > 2$ [9]. In the original correlation, the reference length for Re and $\overline{Nu}$ is the diameter d of the cylinder. With helical coiled resistance wires, however, it seems reasonable to define a reference length which takes into account also the diameter D and the pitch S_C of the helix. In fact, the experimental data collected in this study are satisfactorily represented by the Churchill and Bernstein correlation with a reference diameter d_0 computed from the expression

$$\frac{d_0 - d}{D - d} = \exp\left[1 - \left(\frac{S_C}{d}\right)^n\right] \tag{24}$$

with $n = 1.3$. As can be seen from the plot of Eq. (24) in Fig. 7, for very large values of the S_C/d ratio (when the wire is straightened up) d_0 does not differ much from d while, for S_c/d tending to unity (when the loops form a cylinder of diameter D), d_0 tends to coincide with D. However, only the $2 \leqslant S_C/d \leqslant 4$ range, denoted by the continuous line in Fig. 7, is of practical significance. In this range, the square and triangles correspond to the resistance branches described in Table 1. In accordance with Eq. (24), the definitions: $\overline{Nu} = \bar{\alpha} d_0/\lambda$ and $Re = \bar{u} d_0/\nu$ are adopted in Eq. (23).

It must be remarked that the Churchill and Bernstein correlation was developed for a single isothermal cylinder in cross flow and, thus, caution is required in its use with boundary conditions of uniform heat flux [13], and banks of tubes [3]. In the heaters investigated here, however, variations in the 26

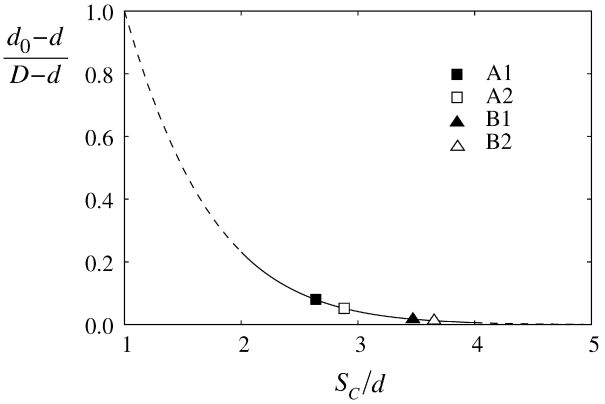

Fig. 7. Dimensionless representation of the d_0 vs. S_C curve: the continuous line denotes the interval of practical interest.

to 65 kW/m^2 interval of the heat flux dissipated by the resistances did not exert any appreciable influence on the measured values of the average convection heat transfer coefficients. The explanation is that the Biot number $Bi = \alpha d/\lambda_w$, based on the diameter and the thermal conductivity of the wire, never exceeded the 0.005 limit. Thus circumferential variations of the surface temperature were negligible, despite the boundary conditions of uniform heat flux. Furthermore, as already pointed out, during preliminary tests no significant changes in the heat transfer performance of the heating branches were induced by reversing their upstream and downstream positions. These preliminary tests were carried out on both heaters A and B, and concerned both branches 1 and 2 operating at the highest and the lowest flow rates. On the basis of Eq. (10), we evaluated the relative differences $(\bar{\alpha} - \bar{\alpha}_R)/\bar{\alpha}$ between heat transfer coefficients in standard and reversed positions. For the whole set of $n = 8$ comparative tests, the averaged value

$$\left|\frac{\bar{\alpha} - \bar{\alpha}_R}{\bar{\alpha}}\right|_{\text{avr}} = \left|\frac{\overline{Nu} - \overline{Nu}_R}{\overline{Nu}}\right|_{\text{avr}} = \frac{1}{n}\sum_{j=1}^{n}\left|\frac{\bar{\alpha} - \bar{\alpha}_R}{\bar{\alpha}}\right|_j \tag{25}$$

and the maximum value

$$\left|\frac{\bar{\alpha} - \bar{\alpha}_R}{\bar{\alpha}}\right|_{\text{max}} = \left|\frac{\overline{Nu} - \overline{Nu}_R}{\overline{Nu}}\right|_{\text{max}} = \max\left|\frac{\bar{\alpha} - \bar{\alpha}_R}{\bar{\alpha}}\right|_j \tag{26}$$

of the relative differences were 1 and 2%, respectively, that is well within the limits of the experimental error. Consequently, no regularity could be claimed to indicate a possible increase of the Nusselt number at the downstream position with respect to the upstream position. On the contrary, the literature suggests that moving a three-row branch of staggered tubes from the upstream to the downstream position in a low Reynolds number flow, induces a relative increase of the Nusselt number of the order of 9% [3, p. 6.32], that is well above the limits of the experimental error. Thus we inferred that wake interactions between coils played a negligible role in our tests. A possible explanation is that, in the heaters investigated here, the percentage of open space between resistance wires is much higher than the percentage of open space between tubes in standard cross-flow heat exchangers. In fact, the ratios S_L/d and S_T/d between longitudinal and transverse distances of the coils and wire diameters are of the order of 20, while the corresponding ratios in standard cross-flow heat exchangers do not exceed 3 [14, p. 379].

5. Results and discussion

Experimental data concerned forced convection heat transfer, in cross flow of air, from the banks of the helical coiled resistance wires described in Table 1. Thermophysical properties used in the calculations were referred to the average fluid temperature defined by Eq. (6). The volume flow rate was varied in the range from 60 to 180 m^3/h, and the corresponding range of Reynolds numbers was $70 \leqslant Re \leqslant 400$. A constant value of the Prandtl number ($Pr \cong 0.71$) was utilized for all the calculations. The bulk temperatures changed from an approximately constant value of 22 °C at inlet, to a maximum value of about 90 °C at outlet (in correspondence with the maximum rated power and the minimum volume flow rate). The average temperature of the coils changed from a minimum value of about 90 °C (in correspondence with the minimum load and the maximum air flow rate), to a maximum value of about 300 °C (in correspondence with the maximum rated power of the heaters and the minimum air flow rate).

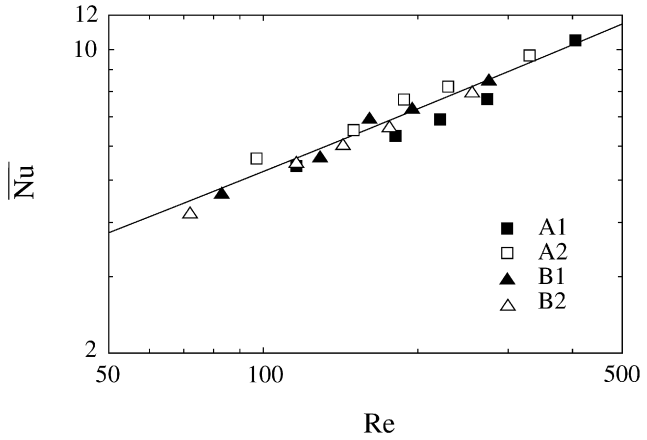

Fig. 8. Experimental (black and white symbols) and predicted (continuous line) average Nusselt numbers vs. the Reynolds number.

In Fig. 8, experimental and predicted values of average Nusselt number $\overline{Nu}$, are shown vs. the Reynolds number, with logarithmic scales on both axes. The predicted values are represented by the continuous line, while results concerning upstream branches, in which the heat flux is lower, are denoted by black symbols, and results concerning downstream branches, in which the heat flux is higher, are denoted by white symbols. As can be seen, no regularity can be detected to indicate that either the heat flux or the position in the bank influence the Nusselt number. In the whole range of Reynolds numbers investigated, the agreement between measured and calculated values is satisfactory. For the whole set of $n = 20$ measuring points, the averaged value

$$|\Delta\overline{Nu}|_{\text{avr}} = \frac{1}{n}\sum_{j=1}^{n}|\Delta\overline{Nu}_j| \tag{27}$$

and the maximum value

$$|\Delta\overline{Nu}|_{\text{max}} = \max|\Delta\overline{Nu}_j| \tag{28}$$

of the deviations are 7 and 12%, respectively, that is well within the ±20% limits of the original Churchill and Bernstein correlation [14, p. 371].

6. Conclusions

It has been shown experimentally that a modified version of the Churchill and Bernstein correlation can satisfactorily predict the average values of the Nusselt number during forced convection heat transfer from banks of helical coiled resistance wires in cross flow. In fact, for the whole set of experimental tests carried out during this study, the maximum and average deviations between experimental and predicted values of the

Nusselt number are 12 and 7%, respectively. It must be pointed out that the modification of the original Churchill and Bernstein correlation, only concerns the definition of a new reference diameter which takes into account the influence of the coil geometry. No modification of the original correlation was needed to account for the boundary conditions of uniform heat flux, possibly because of the small diameter and high thermal conductivity of the resistance wires. Similarly, no modification was needed to account for wake interactions between coils, possibly because of the high percentage of inter-spaces between wires.

References

[1] D. Jones, Ten tips for selecting open-coil, tubular or finned-tubular elements, http://www.indeeco.com, 2004, Tech. rep., Industrial Engineering & Equipment Co.

[2] B.H. Chang, A.F. Mills, Effect of aspect ratio on forced convection heat transfer from cylinders, International Journal of Heat and Mass Transfer 47 (2004) 1289–1296.

[3] A. Zukauskas, Convective heat transfer in cross flow, in: S. Kakac, R.K. Shah, W. Aung (Eds.), Handbook of Single-Phase Convective Heat Transfer, Wiley, New York, 1987 (Chapter 6.3).

[4] M.E. Ali, Experimental investigation of natural convection from vertical helical coiled tubes, International Journal of Heat and Mass Transfer 37 (1994) 665–671.

[5] R.C. Xin, M. Ebadian, Natural convection heat transfer from helicoidal pipes, Journal of Thermophysics and Heat Transfer 12 (1996) 297–392.

[6] M. Ali, Laminar natural convection from constant heat flux helical coiled tubes, International Journal of Heat and Mass Transfer 41 (1998) 2175–2182.

[7] T.J.R.D.G. Prabhanjan, G.S.V. Raghavan, Natural convection heat transfer from helical coiled tubes, International Journal of Thermal Sciences 43 (2004) 359–365.

[8] M.E. Ali, Natural convection heat transfer from vertical helical coils in oil, Heat Transfer Engineering 27 (3) (2006) 79–85.

[9] S.W. Churchill, M. Bernstein, A correlating equation for forced convection from gas and liquids to a circular cylinder in crossflow, Journal of Heat Transfer 99 (1977) 300–306.

[10] M. Hribersek, B. Sirok, Z. Zunic, L. Skerget, Numerical computation of turbulent conjugate heat transfer in air heater, in: Proceedings of the ASME, ZSIS International Thermal Science Seminar II, Bled, Slovenia, American Society of Mechanical Engineers, 2004, pp. 787–792.

[11] E. Doebelin, Measurement Systems: Application and Design, McGraw–Hill, New York, 2004.

[12] G. Comini, Fundamentals of Mechanical and Thermal Measurements, CLEUP, Padua, Italy, 1975 (in Italian).

[13] B.H. Chang, A.F. Mills, Effect of wall thermal boundary condition on heat transfer to separated flow, Journal of Enhanced Heat Transfer 5 (1998) 101–110.

[14] F.P. Incropera, D.P. DeWitt, Fundamentals of Heat and Mass Transfer, Wiley, New York, 1996.